

# Measurement of the half-life of $^{95m}\text{Tc}$ and the $^{96}\text{Ru}(n, x)$ $^{95m}\text{Tc}$ reaction cross-section induced by D–T neutron with covariance analysis

N. Dattathreya<sup>1</sup>, Dr. Arun balaji R<sup>2</sup>, Dr. V.Balaji<sup>3</sup>

<sup>1</sup>Assistant Professor, <sup>2,3</sup> professors

<sup>1,2</sup>Department of Physics, Department of Chemistry  
Bheema Institute of Technology and Science, Adoni

**ABSTRACT:** Using off-line  $\gamma$ -ray spectroscopy in conjunction with the neutron activation approach, the half-life of  $^{95m}\text{Tc}$  and the cross-section of the  $^{96}\text{Ru}(n, x)$   $^{95m}\text{Tc}$  reaction generated by D-T neutrons were determined. The Chinese Academy of Engineering Physics' (CAEP) K-400 neutron generator was used to create the neutron beam from the T (d, n)  $^4\text{He}$  reaction. The observed half-life of  $^{95m}\text{Tc}$  was found to be  $61.88 \pm 0.22$  days by the use of exponential function fitting and a thorough description of the uncertainty evaluation. This is a significant reduction in uncertainty when compared to the currently recommended value. The cross-sections of the  $^{96}\text{Ru}(n, x)$   $^{95m}\text{Tc}$  reaction at the  $13.85 \pm 0.2$ ,  $14.30 \pm 0.2$ , and  $14.72 \pm 0.2$  MeV neutron energies were measured in relation to the  $^{93}\text{Nb}(n, 2n)$   $^{92m}\text{Nb}$  monitor reaction based on the measurement of the  $^{95m}\text{Tc}$  half-life. Covariance analysis was used to carry out a complete uncertainty propagation process taking into account the correlations between various parameters. The cross-sections were then given together with their uncertainties and correlation matrix. Next, theoretically derived values utilizing the TALYS-1.95 and EMPIRE-3.2.3 programs were used to compare the experimentally determined cross-sections with the literature data found in the EXFOR database. Current experimental results are much more accurate with detailed uncertainties and covariance information, which is essential for enhancing the quality of the nuclear database and confirming the theoretical model's dependability.

## 1. INTRODUCTION

Basic nuclear data such as reaction cross-section data induced by neutron and half-life of radionuclides are important in a variety of fields, including accelerator-driven subcritical systems (ADS), reactors, astrophysics, radiation therapy, dosimetry, and so on [1]. In particular, the fast neutron induced reaction cross-section, is crucial for understanding the nuclear phenomena inspent fuel. The sedataare necessary to estimate the nuclear transmutation rates, nuclear heating, and induced radioactivity. Moreover, the experimental crosssections can be used to test the different statistical model codes [2]. The neutron activation method has been widely used for measurements of nuclear reaction cross-sections in these studies. The half-life of the generated nucleus is essential for the activation method since the evaluated crosssection is related to  $T_{1/2}$  of the populated nucleus [3, 4]. Ruthenium is one of the fission products and abundant in the nuclear spent fuel. The half-life of radionuclides produced by irradiation of ruthenium with neutron and the  $(n, x)$  reaction cross-sections of its isotopes are vital in evaluating the radiation safety of nuclear spent fuel.  $^{95m}\text{Tc}$  is one of the products of  $^{96}\text{Ru}(n, x)$  reaction and has a long

half-life. To date, the half-life of  $^{95m}\text{Tc}$  has only been measured by three laboratories, and the uncertainty is very widely spread from 0.13 to 3.28%, as shown in Table 1 [5–7]. Although the uncertainty of the half-life measured by Catterson is far less than the recommended value, the linearization of the exponential decay function is used to analyze data in the literature, and the uncertainty is solely derived from fit uncertainty [5, 6]. Pommé et al. have shown that an incomplete uncertainty estimation based solely on the least-squares fit leads

**Table 1 Half-life of  $^{95m}\text{Tc}$  reported in previous literature**

Author	Detector	$T_{1/2}$ (days)	References
Unik and Rasmussen (1959)	NaI	$61 \pm 2$	[5]
Catterson (2006)	HPGe	$61.95 \pm 0.08$	[6]
Szegedi (2020)	HPGe	$61.96 \pm 0.24$	[7]

to unrealistic values [8]. Szegedi et al. consider both statistical uncertainty and system uncertainty in their measurement, in which the system uncertainty is determined by measuring the half-life of the reference source [7]. Due to the few half-life data at present, the accuracy of uncertainty for half-life measured by Szegedi needs to be verified. Therefore, it is necessary to measure a new half-life of  $^{95m}\text{Tc}$  with a well-documented uncertainty estimation to improve the accuracy of the cross-section.

In addition, only a few studies were conducted on the measurements of activation cross-sections for ruthenium bombarded with neutron, especially in the  $^{96}\text{Ru}(n, x)^{95m}\text{Tc}$  reaction. The latest measured cross-section data of  $^{96}\text{Ru}(n, x)^{95m}\text{Tc}$  reaction around 14 MeV is carried out almost 15 years ago. Besides, the nuclear reaction program of TALYS and EMPIRE codes are developed for the calculation of ground and isomeric states cross-sections in recent years [9]. Thus, new experimental cross-sections are still needed to verify the reliability of these theoretical models. Furthermore, covariance analysis is a mathematical tool that can help to describe the detailed experimental uncertainties with cross-correlation among different measured quantities [10, 11]. The uncertainty accompanied with the cross-section is essential in determining of reasonable margin, which contributes to both safety and economy in nuclear applications [12–14]. If several data points of the activation cross-sections are involved in determination of the quantity of interest, the correlation (covariance) among the data points must also be considered to avoid overestimation or underestimation of the uncertainty in the quantity of interest. Due to this situation, modern evaluation attempts to provide not only the best estimate of the cross-section

but also its uncertainty and covariance describing correlation among cross-sections. However, many prior experiments did not calculate the covariance of  $^{96}\text{Ru}(n, x)^{95\text{m}}\text{Tc}$  reaction cross-section. Considering the above facts, new experimental cross-sections with the covariance analysis are required to verify the reliability and improve the accuracy of these evaluated nuclear data and theoretical models.

In this work, the half-life of  $^{95\text{m}}\text{Tc}$  was measured with the High Purity Germanium (HPGe) detector and the uncertainty was thoroughly discussed. Based on the determination of the  $^{95\text{m}}\text{Tc}$  half-life, the cross-sections of  $^{96}\text{Ru}(n, x)^{95\text{m}}\text{Tc}$  reaction at the  $13.85 \pm 0.2$ ,  $14.30 \pm 0.2$  and  $14.72 \pm 0.2$  MeV neutron energies were measured relative to the  $^{93}\text{Nb}(n, 2n)^{92\text{m}}\text{Nb}$  monitor reaction. In order to improve the accuracy and reliability of the final reaction cross-sections, detailed covariance analysis was performed to estimate the uncertainty of cross-section and the correlation matrix between different reaction cross-sections. Then, theoretical calculations were carried out with the EMPIRE-3.2.3 and TALYS1.95 codes. The experimental results were compared to the existing cross-sections data available in the EXFOR database and the results calculated by different nuclear level density models of TALYS-1.95 and EMPIRE-3.2.3 codes [15–19].

## 2. EXPERIMENT DETAILS

### 2.1 Samples

About 6 g of ruthenium powder of natural isotopic composition (purity 99.95%) was pressed into a pellet (about 20.0 mm in diameter, 1.5 mm in thickness). Monitor foils of natural niobium foils (purity 99.99%, 0.1 mm in thickness) of the same diameter as the pellet were attached in the front and at the back of each ruthenium sample. Three groups of such samples were prepared for irradiation and measurement.

Irradiation was carried out at the K-400 Intense Neutron Generator at the China Academy of Engineering Physics (CAEP) and lasted approximately 17 h with a yield  $\sim 3$  to  $4 \times 10^{10}$  n/(4 $\pi$ s). The deuteron ion beam current was up to 180  $\mu\text{A}$  with an energy of 250 keV. The solid tritium titanium (T-Ti) target used in the generator was approximately 2.59 mg/cm<sup>2</sup> thick. A schematic diagram of sample positions is shown in Fig. 1. The groups of samples were placed at 35°, 75° and 112° relative to the deuteron beam direction and centered around the T-Ti target at a distance of about 4.5 cm. The neutron energy determined by Q equation

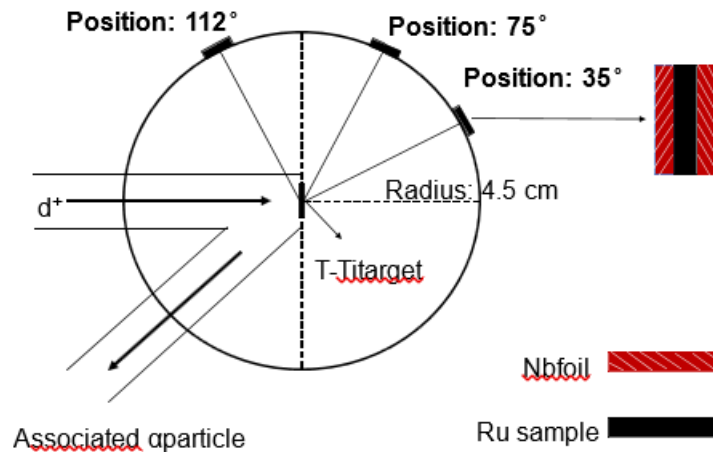


Fig. 1 Schematic diagram of experimental geometry

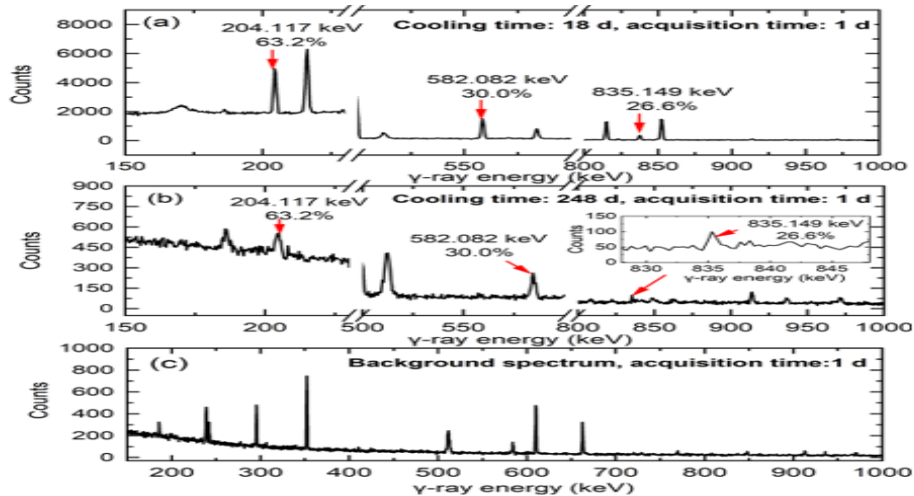


Fig. 2 Background subtracted  $\gamma$  spectra of the activation sample were placed at  $75^\circ$  with different cooling times ( $t_i$ ) were measured using the HPGe detector: a  $t_1$  18 days, b  $t_2$  248 days, and the characteristic  $\gamma$ -ray peaks of  $^{95m}\text{Tc}$  listed in Table 2 were marked; c background spectrum was

$(13.85 \pm 0.20)$  MeV,  $(14.30 \pm 0.20)$  MeV and  $(14.72 \pm 0.20)$  MeV, respectively [20, 21]. The uncertainties in incident neutron energies given above are the quadratic summation of the uncertainties caused by the energy straggling of incident deuteron ion in the T-Ti target and the angle divergence from target to samples [22]. During irradiation, the variation of the neutron yield was monitored by accompany-

ing  $\alpha$  particles to make corrections for the fluctuation in the neutron flux.

### 2.3 Gamma spectrum measurement

After completion of the neutron irradiation, the samples were cooled about 18 days, the  $\gamma$ -rays emitted by the activation sample at different cooling times were obtained from continuous off-line measurements using a lead-shielded HPGe detector (ORTEC, USA). The signals from the detector preamplifier were first shaped (the shaping time was set to 6  $\mu$ s), and the data were collected by ORTEC MAESTRO software, which provides precise deadtime information.

Before irradiation, the efficiency of the HPGe detector was calibrated using a  $^{152}\text{Eu}$  standard sources with known activity. The relative efficiency of the detector was 68%, and the energy resolution was 1.82 keV (FWHM) at 1.33 MeV of  $^{60}\text{Co}$ . In order to measure the half-life accurately, a total of 21 spectra were collected with different cooling times, and the individual spectrum was recorded for 1 day. The measurement covered approximately 4 half-lives of  $^{95}\text{mTc}$ . The upper limit of dead time was set at less than 0.12% for each measurement (especially for the first running). The dead time uncertainty component was propagated using the initial measurement recorded dead time of 0.12% [23, 24]. In addition, the probability of pulse pile-up was calculated using the Poisson distribution [25]. It was calculated that the probability of no pulse pile-up in all measured energy spectra was greater than 99.97%, and the probability of one pulse pile-up was less than 0.03%. When the probability of pulse pile-up is less than 1%, the influence on the count of the  $\gamma$  characteristic peaks is insignificant and can therefore be ignored. Figure 2 shows the background spectrum and the typical background subtracted  $\gamma$  spectra acquired from the irradiated samples placed at  $75^\circ$ . The details of the nuclear decay data and their uncertainties used in the present experiment are given in Table 2.

## 3. DATA ANALYSIS

### 3.1 Estimation of half-life uncertainty propagation

The correct propagation of uncertainty components is an important issue in the measurement of radionuclide half-life [8]. For normally distributed random fluctuations, a rigorous uncertainty propagation factor can be derived from linear regression formulas. Assuming that the relevant standard uncertainty  $\sigma_i$  for each activity measurement  $A_i$  is known, the uncertainty of the least-squares solution for the half-life is expressed as the following equation [28]

$$\frac{\sigma_{T_{1/2}}}{T_{1/2}} = \frac{1}{\lambda} \frac{\sigma_{A_w}}{\sqrt{\sum_{i=1}^n A_i^2}} \quad (1)$$

Where  $\text{var}(t)$  represents the variance of the measurement start

times, and  $\frac{\sigma_{A_w}}{A_w} = \frac{1}{\sqrt{\sum_{i=1}^n (\sigma_{A_i})^{-2}}} A_i^{-1/2}$  is the expected relative uncertainty on the weighted average activity.



For a series of activity measurements with the same relative uncertainty  $\sigma_i$   $\sigma_A$  performed equidistant in time over a total duration  $T$ , Eq. (1) can be derived as Eq. (2)

$$(2) \sigma_T^{1/2} = \frac{2}{\lambda T} \sqrt{\frac{3(n-1)\sigma_A T_{1/2}}{n(n+1)A}}$$

in which,  $T$  is the duration of the campaign,  $\sigma_A$  is the measure of the uncertainty for a typical activity measurement. The formula does not apply to medium and long-term variations but only to short-term fluctuations since it implicitly assumes that the data are independent [8]. Based on the assumption that

**Table 2** Nuclear decay data and their uncertainties used in the present experiment [26, 27]

Reaction	Abundance of target isotope (%)	Mode of decay (%)	Half-life of product (days)	$E_\gamma$ (keV)	$I_\gamma$ (%)
$^{96}\text{Ru} (n, x)$	5.54	EC (96.12)	61.88 ± 0.22	204.117	63.20 ± 0.80
		$^{95\text{m}}\text{Tc}$	IT (3.88)	582.082	30.20 ± 0.40
				835.149	26.60 ± 0.40
$^{95}\text{Nb} (n, 2n)$	100	EC (100)	10.15 ± 0.02	934.440	99.15 ± 0.04
		$^{92\text{m}}\text{Nb}$			

the relative influence of a measurement on the fitted half-life is proportional to the time difference with the middle of the campaign and data points being scattered roughly uniformly in time over the period  $T$ , a similar approximating formula was obtained [8].

$$\frac{\sigma_T}{T} \approx \frac{2}{\lambda T} \sqrt{\frac{2}{n+1} \frac{\sigma_A}{A}} \quad (3)$$

It is crucial to apply independent uncertainty propagation according to the ‘frequency’ of the uncertainty components. In the Eqs. (2) and (3), the parameter  $n$  is the frequency of the occurrences of the uncertainty component [12, 13]. For high frequency components,  $n$  is set equal to the number of measurements. For medium frequency components,  $n$  is set equal to the number of periods covered by the measurement campaign. For low frequency components,  $n = 1$  is selected by default. Using Eqs. (2) and (3), a realistic uncertainty can be calculated.

### 3.2 Efficiency calibration of the HPGe detector with uncertainty

The standard  $^{152}\text{Eu}$  point source of known activity was used for calibration to obtain the efficiency of the HPGe detector [29, 30]. The nine  $\gamma$ -ray energies of standard  $^{152}\text{Eu}$  source considered are 121.770 keV, 244.830 keV, 344.930 keV, 412.050 keV, 780.520 keV, 868.940 keV, 1113.050 keV, 1299.210 keV and 1407.440 keV.

$$\varepsilon = \frac{C}{A_0 I_\gamma e^{-\lambda t}} \quad (4)$$

where  $\varepsilon$  is the efficiency of the detector;  $C$  is the detected characteristic  $\gamma$ -ray counts measured in time  $t$ ;  $I_\gamma$  is the  $\gamma$ ray abundance;  $A_0$  is the activity of the  $^{152}\text{Eu}$  point source of source calibration;  $T_{1/2}$  is the half-life of radioactive nuclei;  $t$  is the time elapsed between source and detector calibration. In Eq. (4), the parameters  $t$  was measured without any uncertainty, therefore the efficiency is considered to be a function of these four attributes i. e.  $\varepsilon = \varepsilon(C, I_\gamma, A_0, T_{1/2})$ . There is no association among the four traits since they are all measured independently. The details procedure to estimate the covariance matrix  $V_\varepsilon$  is given in Refs. [30, 31]. In order to obtain the most accurate results, the efficiency calibration curve was fitted to a polynomial function [1, 30–32]. The linear parametric model of order  $m$  and estimated fitting parameters  $p_m$  can be represented as  $\ln \varepsilon = p_1 + p_2(\ln E) + p_3(\ln E)^2 + \dots + p_m(\ln E)^{m-1}$  (5)

The corresponding linear model of the above equation can be represented in matrix form as  $Z \approx AP$ , where  $Z_i = \ln \varepsilon_i$  is a column matrix.  $P$  is the column matrix of parameters  $p_m$  to be estimated.  $A$  is a matrix of natural logarithmic of  $\gamma$ -lines  $E_i$ .

A good fit measuring the consistency of the data is tested by Chi square statistic. The best quality of the fit is achieved for  $m = 2$ , with  $\chi^2 = 1$ . The polynomial function is given below:

$$\ln \varepsilon = -5.331079 - 0.661669 \ln E \quad (6)$$

By substituting  $\gamma$ -ray energies in Eq. (6), the detection efficiencies of the characteristic  $\gamma$ -rays emitted by  $^{95}\text{mTc}$  and  $^{92}\text{mNb}$  are obtained. The covariance matrix  $V_\varepsilon$  at the characteristics  $\gamma$ -rays of the reaction products  $^{95}\text{mTc}$  and  $^{92}\text{mNb}$  is determined by equation of Refs. [30, 31]. And the Table 3 presents the estimation of efficiencies of the detector corresponding to the characteristic  $\gamma$ -ray energies of reaction products along with the correlation matrix. The estimated efficiencies are used for further cross-sections calculation.

### 3.3 Determination of the $^{96}\text{Ru}$ (n, x) $^{95}\text{mTc}$ reaction cross-sections and corresponding uncertainty

The measured  $^{96}\text{Ru}$  (n, x)  $^{95}\text{mTc}$  reactions cross-section was derived with the monitor cross-section by activation formula [31]:

**Table 3** Interpolated detector efficiencies of the radionuclide with its correlation matrix

Type of reaction	$E_\gamma$ (keV)	Efficiency	Correlation matrix			
$^{96}\text{Ru}$ (n, x) $^{95}\text{mTc}$	204.117	$0.01385 \pm 0.00014$	1			
	582.082	$0.00692 \pm 0.00019$	0.83194	1		
	835.149	$0.00545 \pm 0.00019$	0.79885	0.99836	1	
$^{93}\text{Nb}$ (n, 2n) $^{92}\text{mNb}$	934.440	$0.00506 \pm 0.00019$	0.79064	0.99750	0.99990	1

$$\sigma_x \sigma_m = \frac{C_x \lambda_x a_m N_m I_{\gamma(m)} \epsilon_m f_m}{C_m \lambda_m a_x N_x I_{\gamma(x)} \epsilon_x f_x} \times \frac{C_{attn_x}}{C_{attn_m}} \quad (7)$$

where  $\sigma$  represents the cross-section and the subscript m and x represent the monitor reaction and measured reaction, respectively; C is counts of characteristic  $\gamma$ -peak;  $\lambda$  is the decay constant; a is the abundance of the target nuclei; N is the number of atoms;  $I_\gamma$  summarized in Table 2 is the  $\gamma$ -ray abundance;  $\epsilon$  is the full-energy peak efficiency; f is the time factor, given by  $(1 - e^{-\lambda T})(1 - e^{-\lambda t})$ , T is the irradiation time, t is the cooling time, and t is the measurement time;  $C_{attn}$  is the total correction factor of the counting process, given by  $C_{attn} = FS * FC * F_g$  (FS, FC,  $F_g$  are the self-absorption correction factor, cascade coincidence correction factor and geometric correction factor, respectively).

The uncertainty propagation in the measured crosssections was analyzed by considering the fractional uncertainty in various attributes, i.e., timing factor ( $f_x, f_m$ ), efficiency ( $\epsilon_x, \epsilon_m$ ),  $\gamma$ -ray intensity ( $I_\gamma(x), I_\gamma(m)$ ), isotopic abundance of the sample nuclei ( $\eta$ ), number of atoms ( $N_x, N_m$ ),  $\gamma$ -ray characteristic peak counts ( $C_x, C_m$ ) and monitor reaction cross-section ( $\sigma_m$ ). The uncertainties in T, t, and t were too small to be incorporated in the uncertainty of the final reaction cross-sections. As in the case of efficiency, the partial uncertainty in the cross-section at neutron energy  $E_i$  due to attribute q, except for the time factor  $f_x$  is propagated as

$$\delta(\sigma_j, E_i)_q = \left| \frac{\partial \sigma_j}{\partial x_q} \right| \delta x_q \quad (8)$$



whereas the uncertainty in time factor,  $f_j$  is propagated as

$$\delta_{(\sigma_j, E_i)\lambda_j} = \left| \frac{\sigma_j}{\lambda_j} - \frac{\sigma_j}{f_j} \times \frac{\partial f_j}{\partial \lambda_j} \right| \delta \lambda_j \quad (9)$$

Hence, the uncertainty in the final cross-section of this work is calculated as

$$\delta \sigma_j = \sqrt{\sum_1^n \delta_{(\sigma, E_i)j}^2 + \sum_1^n \delta_{(\sigma, E_i)Nb}^2 + 2 \sum \delta_{(\sigma, E_i)\epsilon_j} \text{Corr}(\epsilon_j, \epsilon_{Nb}) \delta_{(\sigma, E_i)\epsilon_{Nb}}} \quad (10)$$

The final covariance matrix in the cross-section is obtained by using the following equation:

$$C^{\sigma} = \sum \delta_{(\sigma, E_i)} (M_{\sigma})_{ij} \delta_{(\sigma, E_j)} \quad (11)$$

#### 4. THEORETICAL CALCULATION

The mutual verification between theory and experiment is critical for obtaining reliable and accurate nuclear data. Based on this, theoretical nuclear codes like EMPIRE and TALYS have been used to conduct the calculations of crosssections. The theoretical calculations for  $^{96}\text{Ru}$  (n, x)  $^{95m}\text{Tc}$  reaction were performed by using the statistical nuclear reaction model codes TALYS-1.95 and EMPIRE-3.2.3 [30, 31]. The calculations are based on different mechanisms of the nuclear reactions which vary with the incident energy. Three major reaction mechanisms, including direct reaction (DI), pre-equilibrium emission (PE), and compound nucleus (CN), are considered in these codes. To estimate contributions from all such mechanisms, the codes incorporate various nuclear models that use the different sets of optical model parameters and level density. The contribution from all the three mechanisms determines the total reaction cross-section. The theoretical calculations are carried out by employing the optimum combination of input parameters, and their values obtained for various models and parameters that reproduce the most satisfactory results compared to the current experimental data and all the available existing experimental data reported in the EXFOR database.

##### 4.1 TALYS-1.95 calculation

TALYS is a nuclear reaction program that predicts the nuclear reaction of target nuclides with nuclear mass 12 or heavier, induced by particles of energy ranging from 1 keV to 200 MeV. The nuclear reaction models of optical model, pre-equilibrium reactions, compound reactions and level densities are all contained in the TALYS-1.95 code. In

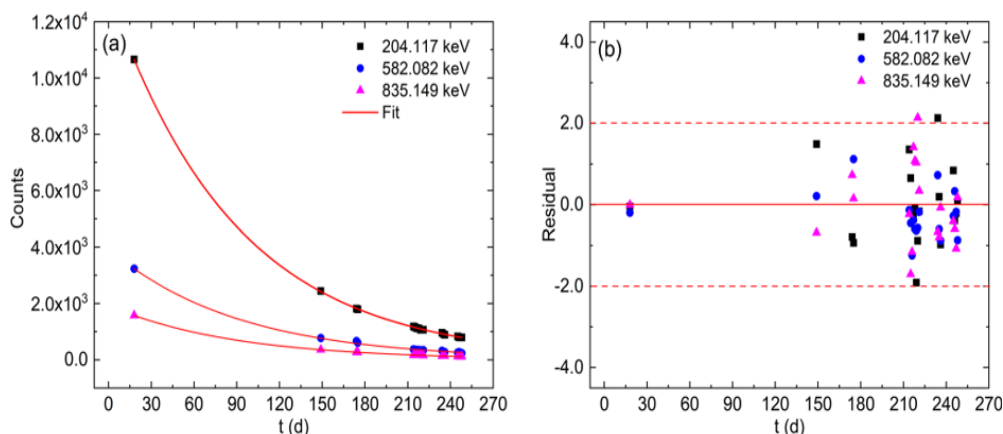


Fig. 3 a The decay curve between the counts and  $t$ . b Normalized residuals of the measured  $^{95m}\text{Tc}$  count versus the fitted exponential decay curve. The residuals show no obvious auto-correlation and seem randomly distributed, mostly within two standard uncertainties.

recent years, some literature considered that nuclear level density play an important role in proton or neutron induced reactions at low and medium energy range [33–36]. Nuclear level density (NLD) is the number of excited levels per energy interval ( $dN/dE$ ) close to the excitation energy. The excited nuclear levels are discrete at low energies; however, they approach a continuum as the excitation energy increases. Therefore, a nuclear model of calculating level density is needed in the continuum energy regime. An accurate and reliable description of the excited levels of a nucleus at both low and high excitation energy regions is necessary for testing the quality of a reaction model used for the calculation of cross-sections [3, 37]. In order to understand the effect of nuclear level density model on neutron induced reactions, theoretical calculations are carried out using the TALYS-1.95 code with default parameters, and only these selected level density parameters are adjusted. The detailed result was present in Fig. 5.

#### 4.2 EMPIRE-3.2.3 calculation

EMPIRE is a program for calculating nuclear reactions, including a variety of theoretical models of nuclear reactions. The EMPIRE-3.2.3 was used for estimating the crosssection of  $^{96}\text{Ru}(n, x)^{95m}\text{Tc}$  reaction. In EMPIRE, the description of the compound level density parameter was carried out according to the Gilbert–Cameron model (LEV DEN 0), while the transmission coefficients were calculated by the spherical optical model using the ECIS-06 code with the global optical model potential, proposed by Koning and Delaroche for neutrons, taken from RIPL-3 library no. 204 Refs. [38, 39]. The statistical Hauser-Feshbach model was used for calculating the compound nucleus contribution [40]. For pre-equilibrium emission, the classical exciton model was used by means of the PCROSS code that calculates the pre-equilibrium contribution with the default mean free path

**Table 4 The half-lives of  $^{95m}\text{Tc}$  measured in this work**

Isotope	$E_{\gamma}$ (keV)	$T_{1/2}$ (d)	$\chi^2$
$^{95m}\text{Tc}$	204.117	62.17	0.9459
	582.082	62.06	0.9501
	835.149	61.42	0.9505

multiplier (PCROSS 1.5). The detailed result was present in Fig. 5.

## 5. RESULTS AND DISCUSSION

### 5.1 Half-life of $^{95m}\text{Tc}$

The  $\gamma$ -ray characteristic peaks of  $^{95m}\text{Tc}$  used in the analysis and corresponding intensities are summarized in Table 2. The counts of  $\gamma$  characteristic peak are fitted with an exponential function by minimizing the squared values of the variance weighted residuals [21]. The fitting curve passes through the experimental points very well with a correlation coefficient  $R \approx 1.0$ , implying that the  $\gamma$ -ray spectra are in a stable condition during the measurement time of 4 half-lives. The fitting residuals presented in Fig. 3 show the majority of data is in the range of  $(-2, 2)$ . The measured half-life of  $^{95m}\text{Tc}$  and the  $\chi^2$  value refers to the exponential fit are shown in Table 4. As can be seen, the values derived from the different  $\gamma$ -transitions are in good agreement. The final half-life of  $^{95m}\text{Tc}$  is taken as the weighted average of the above three values, which is 61.88 days. The weight for each half-life is determined using the high-frequency uncertainty in Table 5.

The uncertainty components are evaluated in accordance with Pommé by taking into account the high-, medium and low-frequency instabilities contributions, and combining these in quadrature to determine the standard uncertainty of the  $^{95m}\text{Tc}$  half-life [8]. The evaluation of uncertainty is presented in Table 5. The high frequency instabilities component is comprised of the standard deviation of the residuals from the least squares fit. This is determined to be 0.22%. The medium frequency instabilities component of the uncertainty is the trend of the residual, which is identified as 0.06%. The low frequency instabilities component of uncertainty are not visible in the residual plot and therefore an attentive analysis needs to be performed. The background subtraction and dead time correction are considered as low frequency components of the uncertainty. In this work, a conservative approach is used for the analysis part of the low frequency instability components, therefore  $n$  set equal to 1. The total uncertainty is 0.35%, as

outlined in Table 5. The final result in this experimentshowedthatthehalf-lifeof  $^{95m}\text{Tc}$  is  $61.88 \pm 0.22$  days.

In conclusion, the measured half-life of  $^{95m}\text{Tc}$  is presented in Fig. 4 along with the previous literature values, where the data represented by the green line in the figure is from the NNDC database [5–7,26]. As shown in Fig. 4, the uncertainty of result is greatly reduced compared with the currently recommended value. The experiment and ensuing uncertainty evaluation are discussed in detail in this work. In addition, the present results further confirm that the earlier results published by Szegedi et al. to be correct and credible [7]. It provides more accurate and reliable half-life fundamental data for applications using an activation method, such as the calculation of the  $^{96}\text{Ru} (n, x) ^{95m}\text{Tc}$  reaction cross-sections.

## 5.2 Cross-section of $^{96}\text{Ru} (n, x) ^{95m}\text{Tc}$ reaction

Based on the half-life of  $^{95m}\text{Tc}$  determined in this measurement,  $^{96}\text{Ru} (n, x) ^{95m}\text{Tc}$  reaction cross-sections have been measured relative to the monitor cross-section of  $^{93}\text{Nb} (n, 2n) ^{92m}\text{Nb}$  at the  $13.85 \pm 0.2$ ,  $14.30 \pm 0.2$  and  $14.72 \pm 0.2$  MeV

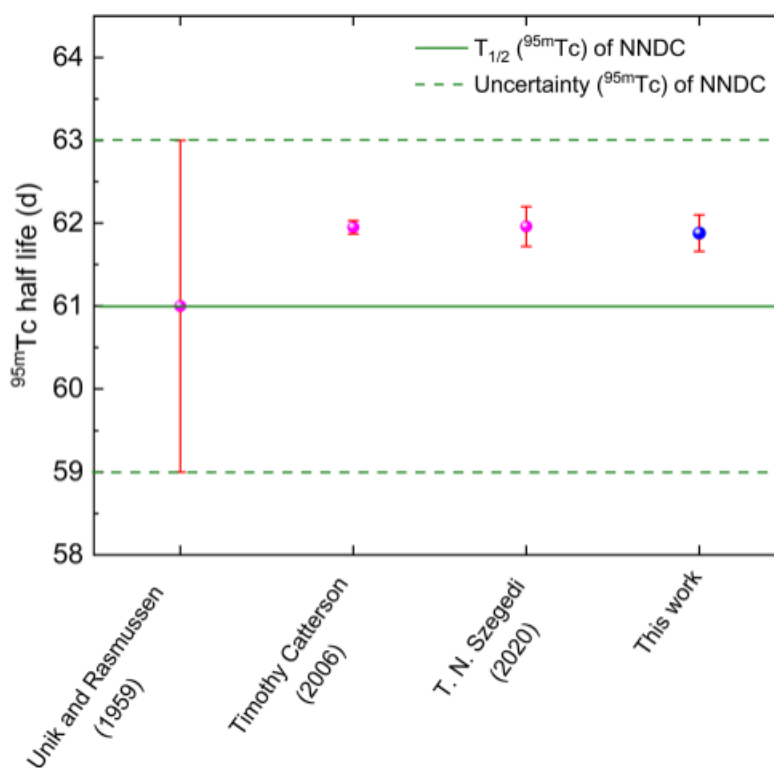


**Fig. 4 The half-life of  $^{95m}\text{Tc}$  calculated in this work compared to the values previously reported**

**Table 5 Uncertainty evaluation for the half-life of  $^{95m}\text{Tc}$ , expressed as relative standard uncertainty**

Components	$\frac{\sigma_A}{A}$ (%)	<del>Propagation factor</del>	$\frac{\sigma_{T_{1/2}}}{T_{1/2}}$ (%)	<u>Total</u> (%)
<i>High frequency</i>				0.35
Standard deviation of residuals	0.22	0.23	0.05	
<i>Medium frequency</i>				
Trends in residuals	0.06	0.23	0.01	
<i>Low frequency</i>				
Background subtraction	0.47	0.72	0.34	
Dead time	0.12	0.72	0.01	

neutron energies using Eq. (7). The counting of all the irradiated samples has been measured with the same detector system, therefore all the reaction cross-sections are correlated with the efficiency of the HPGe detector. Besides, for the calculation of uncertainty in measured cross-sections and its covariance matrix, the counts of the  $\gamma$ -ray spectra and other parameters with definite uncertainties are also taken into consideration. The fractional uncertainties from all these parameters between different reaction cross-sections are summarized in Table 6. The correlations observed between different attributes are also presented in the last column of Table 6. Based on these fractional uncertainties and correlations, the cross-sections with their uncertainties and correlation matrix are presented in Table 7. The final uncertainty determined in the  $^{96}\text{Ru}(n, x)^{95m}\text{Tc}$  reaction cross-section is determined as 2.54–2.76%.

In Fig. 5, the cross-sections of  $^{96}\text{Ru}(n, x)^{95m}\text{Tc}$  are compared with the available literature data in the EXFOR

**Table 6** Fractional uncertainties and correlations in various attributes of measured reactions, the efficiencies and  $\gamma$ -ray abundances of  $^{92m}\text{Nb}$  are calculated at  $E_\gamma = 934.440$  keV

$E_\gamma$ (MeV)	$E_\gamma$ (keV)	x	$N_{\text{Tc}}$	$N_{\text{Nb}}$	$\epsilon_{\text{Tc}}$	$I_{\text{Nb}}$	$\epsilon_{\text{Tc}}$	$\epsilon_{\text{Nb}}$	$I_{\text{Tc}}$	$I_{\text{Nb}}$	$\sigma_{\text{Nb}}$	$C_{\text{Tc}}$	$C_{\text{Nb}}$
13.85	204.117	1	2.0207E-03	2.0450E-02	1.2818E-04	2.3148E-04	4.6230E-03	1.6591E-02	5.6841E-04	1.8333E-04	0.4544	2.8739E-07	2.8675E-07
	582.082	2	1.9650E-03	2.0450E-02	1.2043E-04	2.3148E-04	1.2115E-03	1.6591E-02	5.8223E-04	1.8333E-04	0.4544	2.3988E-06	2.8675E-07
	835.149	3	1.9663E-03	2.0450E-02	1.2051E-04	2.3148E-04	1.5035E-03	1.6591E-02	9.8561E-04	1.8333E-04	0.4544	4.0909E-06	2.8675E-07
14.30	204.117	4	2.4033E-03	2.0680E-02	1.4872E-04	5.1596E-04	5.4984E-04	1.6772E-02	6.7604E-04	1.8540E-04	0.4596	1.9586E-07	3.7806E-07
	582.082	5	2.3705E-03	2.0680E-02	1.4669E-04	5.1596E-04	1.4615E-03	1.6772E-02	7.0237E-04	1.8540E-04	0.4596	1.5854E-06	3.7806E-07
	835.149	6	2.6243E-03	2.0680E-02	1.6240E-04	5.1596E-04	2.0066E-03	1.6772E-02	1.3154E-03	1.8540E-04	0.4596	2.7508E-06	3.7806E-07
14.72	204.117	7	2.8009E-03	2.0567E-02	1.7182E-04	5.3620E-04	6.4081E-04	1.6687E-02	7.8789E-04	1.8439E-04	0.4571	7.1294E-07	4.1697E-07
	582.082	8	2.6981E-03	2.0567E-02	1.6550E-04	5.3620E-04	1.6635E-03	1.6687E-02	7.9942E-04	1.8439E-04	0.4571	6.0182E-06	4.1697E-07
	835.149	9	2.8965E-03	2.0567E-02	1.7768E-04	5.3620E-04	2.2147E-03	1.6687E-02	1.4519E-03	1.8439E-04	0.4571	9.9149E-06	4.1697E-07
Correlation			1, 2, 3 fully correlated, 4, 5, 6 fully correlated, 7, 8, 9 fully correlated	1, 2, 3 fully correlated, 4, 5, 6 fully correlated, 7, 8, 9 fully correlated	1, 2, 3 fully correlated, 4, 5, 6 fully correlated, 7, 8, 9 fully correlated	Fully correlated	Correlated	1, 2, 3 fully correlated, 4, 5, 6 fully correlated, 7, 8, 9 fully correlated	1, 4, 7 fully correlated, 2, 5, 8 fully correlated, 3, 6, 9 fully correlated	Fully correlated	1, 2, 3 fully correlated, 4, 5, 6 fully correlated, 7, 8, 9 fully correlated	Uncorrelated	1, 2, 3 fully correlated, 4, 5, 6 fully correlated, 7, 8, 9 fully correlated

**Table 7** The measured reaction cross-sections with uncertainty and correlation

$E_{\text{th}}$ (MeV)	$E_\gamma$ (keV)	Cross-section(Barns)	Correlation matrix
13.85 ± 0.20204	1170.04490	± 0.001181.0000	
	582.0820.04367	± 0.001130.09081.0000	
	835.1490.04370	± 0.001120.09670.28601.0000	
14.30 ± 0.20204	1170.05341	± 0.001440.04610.09080.37431.0000	
	582.0820.05268	± 0.001460.09080.25830.28600.09081.0000	
	835.1490.05832	± 0.001580.09670.28600.31780.09670.28601.0000	
14.72 ± 0.20204	1170.06224	± 0.001640.04610.47260.74650.04610.09080.09671.0000	
	582.0820.05996	± 0.001540.09080.25830.28600.09080.25830.28600.09081.0000	
	835.1490.06437	± 0.001630.09670.28600.31780.09670.28600.31780.09670.28601.0000	

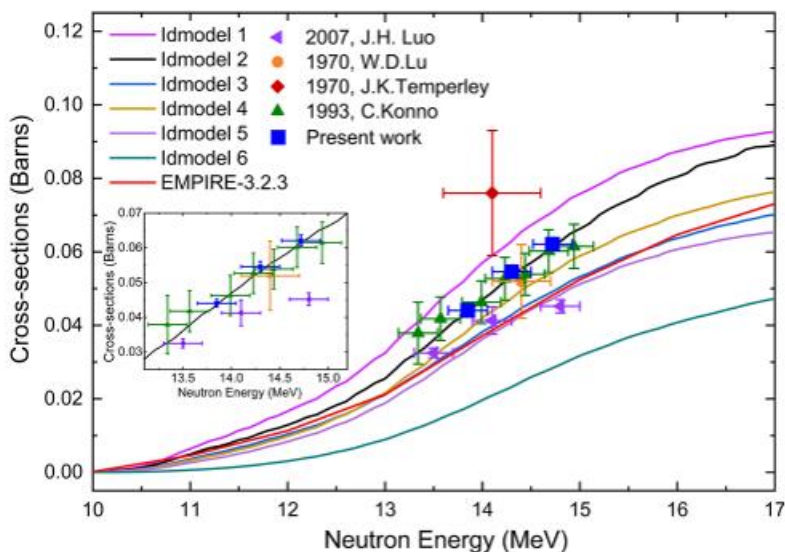


Fig. 5 Cross-section of  $^{96}\text{Ru}(n, x)^{95m}\text{Tc}$  reaction measured in present work and comparative studies with the existing experimental crosssection data at different neutron energies and theoretically calculated results from the TALYS-1.95 and EMPIRE-3.2.3

database [15–18]. The measurements of 13–15 MeV neutron energies show discrepancies between the data measured by different groups. Figure 5 reveals that the present data are consistent with the data of Lu et al. [15] and Konno et al. [17] within the experimental uncertainties, and a considerable improvement in accuracy was achieved [15–18]. Considering the correlation of uncertainties arising from various sources of experimental error, the final uncertainty results will be evaluated more accurately [30].

In addition, the excitation function of the  $^{96}\text{Ru}(n, x)^{95m}\text{Tc}$  reaction is calculated theoretically through the TALYS-1.95 code and EMPIRE-3.2.3 with default parameters. In Fig. 5, shapes of the excitation curves calculated using the TALYS1.95 (Idmodels 1–6) and EMPIRE-3.2.3 exhibit a trend similar to the present data set, which increases with increasing neutron energy around 14 MeV. However, the result calculated by Idmodel 6 in TALYS-1.95 significantly underestimates the excitation function. The excitation functions calculated by the level density model of Idmodel 2 in TALYS-1.95 are in good agreement with experimental data in shape and magnitude. While, Idmodel 3 in TALYS-1.95 and EMPIRE3.2.3 are consistent with the results reported by Luo et al. within the experimental uncertainties. Therefore, it also shown that more experimental data are still needed to verify the accuracy of theoretical calculations, especially for energy above 15 MeV. The present results contribute to improving the knowledge of the cross-sections and optimizing the input parameters of model, which is essential to support nuclear technology developments.

## 6. CONCLUSIONS

This work used the most recent decay data to measure the half-life of  $^{95m}\text{Tc}$  and the cross-section of the  $^{96}\text{Ru} (n, x) ^{95m}\text{Tc}$  reaction induced by  $13.85 \pm 0.2$ ,  $14.30 \pm 0.2$ , and  $14.72 \pm 0.2$  MeV. The uncertainty was thoroughly explored. The most recent data were exponentially fitted, and the uncertainty was carefully assessed. The accurate half-life of  $^{95m}\text{Tc}$  was found to be  $61.88 \pm 0.22$  days. This uncertainty is substantially lower than the suggested value  $T_{1/2} 61 \pm 2$  days in NNDC, which further supports the accuracy of the findings previously released by Szegedi et al. For applications utilizing an activation approach, such the computation of the  $^{96}\text{Ru} (n, x) ^{95m}\text{Tc}$  reaction cross-section, it offers a more precise and dependable half-life. The covariance matrix methodology was utilized for both the uncertainty measurement of the  $^{96}\text{Ru} (n, x) ^{95m}\text{Tc}$  reaction cross-sections and the efficiency calibration of the HPG detector. The range of 2.54–2.76% is where the uncertainties in the measured cross-sections are located. The available literature data in the EXFOR database was then compared with the experimental results. Furthermore, the current measured cross-sections were also replicated with the programs EMPIRE-3.2.3 and TALYS-1.95 from the theoretical nuclear reaction model. Then, the nuclear model with the TALYS-1.95 code demonstrated that the cross-section for the  $^{96}\text{Ru} (n, x) ^{95m}\text{Tc}$  reaction is suitable for the back-shifted Fermi gas model (ldmodel 2). However, the excitation function curve is underestimated in the data produced by EMPIRE-3.2.3. Thus, more experimental data are still required, particularly for energies beyond 15 MeV, to confirm the accuracy of theoretical estimates. Current experimental results, which include comprehensive uncertainties and covariance data, can be used to validate nuclear reaction codes and guarantee the security of nuclear technology advancements.

Recognitions The Chinese Academy of Engineering Physics' K-400 Intense Neutron Generator staff provided excellent neutron generator operation and other support during the experiment, for which the authors are appreciative. The National Natural Science Foundation of China provided funding for this work (Grant No. 11975113).

Statement of Data Availability There are no corresponding data for this manuscript, or the data will not be deposited. [Authors' comment: This published publication contains all the data generated during this investigation.]

## References

- [1] A. Gandhi, A. Sharma, A. Kumar, Phys. Rev. C 102, 014603 (2020)
- [2] L.A. Bernstein et al., Annu. Rev. Nucl. Part. S 69, 109 (2019)
- [3] J.H. Luo, L. Jiang, Eur. Phys. J. A 55, 25 (2019)
- [4] T. Hayakawa et al., Phys. Rev. C 74, 065802 (2006)
- [5] J.P. Unik, J.O. Rasmussen, Phys. Rev 115, 1687 (1959)
- [6] T. Catterson, D.J. Van Dalsem, Appl. Radiat. Isot 64, 1425 (2006) 7. T. Szegedi et al., Eur. Phys. J. A 56, 1 (2020)